



ISSN 2056-9890

Crystal structure, Hirshfeld surface analysis, DFT and molecular docking investigation of 2-(2-oxo-1,3-oxazolidin-3-yl)ethyl 2-[2-(2-oxo-1,3-oxazolidin-3-yl)ethoxy]quinoline-4-carboxylate

Younos Bouzian,^a Cemile Baydere,^{b*} Necmi Dege,^b Nouredine Hamou Ahabchane,^a Joel T. Mague,^c Abdulmalik Abudunia,^{d*} Khalid Karrouchi^e and El Mokhtar Essassi^a

Received 2 November 2020

Accepted 7 December 2020

Edited by M. Weil, Vienna University of Technology, Austria

Keywords: crystal structure; Covid-19; DFT; Hirshfeld surface analysis; oxazolidine; quinoline; Molecular docking.

CCDC reference: 2048734

Supporting information: this article has supporting information at journals.iucr.org/e

^aLaboratory of Heterocyclic Organic Chemistry URAC 21, Pole of Competence, Pharmacochemistry, Av Ibn Battouta, BP 1014, Faculty of Sciences, Mohammed V, University, Rabat, Morocco, ^bDepartment of Physics, Faculty of Arts and Sciences, Ondokuz Mayıs University, 55139-Samsun, Turkey, ^cDepartment of Chemistry, Tulane University, New Orleans, LA 70118, USA, ^dDepartment of Pharmacology, Faculty of Clinical Pharmacy, University of Medical and Applied Sciences, Yemen, and ^eLaboratory of analytical Chemistry and Bromatology, Faculty of Medicine and Pharmacy, Mohammed V University, Rabat, Morocco. *Correspondence e-mail: cemle28baydere@hotmail.com, abdulmalikabudunia@gmail.com

In the molecular structure of the title compound, C₂₀H₂₁N₃O₇, the quinoline ring system is slightly bent, with a dihedral angle between the phenyl and the pyridine rings of 3.47 (7)°. In the crystal, corrugated layers of molecules extending along the *ab* plane are generated by C—H···O hydrogen bonds. The intermolecular interactions were quantified by Hirshfeld surface analysis and two-dimensional fingerprint plots. The most significant contributions to the crystal packing are from H···H (42.3%), H···O/O···H (34.5%) and H···C/C···H (17.6%) contacts. Molecular orbital calculations providing electron-density plots of the HOMO and LUMO as well as molecular electrostatic potentials (MEP) were computed, both with the DFT/B3LYP/6–311 G++(d,p) basis set. A molecular docking study between the title molecule and the COVID-19 main protease (PDB ID: 6LU7) was performed, showing that it is a good agent because of its affinity and ability to adhere to the active sites of the protein.

1. Chemical context

Quinoline and its derivatives have attracted the interest of synthetic and biological chemists because of their interesting chemical and pharmacological properties (Chu *et al.*, 2019), including antibacterial (Bouzian *et al.*, 2020), anticancer (Tang *et al.*, 2018), antitubercular (Xu *et al.*, 2017), anti-COVID19 (Gao *et al.*, 2020), antimalarial (Hu *et al.*, 2017), anti-leishmanial (Palit *et al.*, 2009) and anti-inflammatory (Pinz *et al.*, 2016) activities. Furthermore, many studies have shown that quinoline derivatives are good corrosion inhibitors (Douche *et al.* 2020).

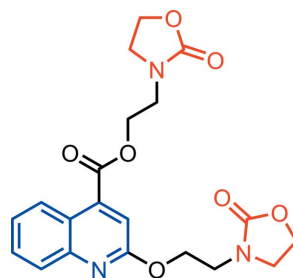
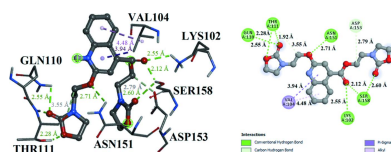


Table 1
Hydrogen-bond geometry (Å, °).

$D-H\cdots A$	$D-H$	$H\cdots A$	$D\cdots A$	$D-H\cdots A$
C2—H2···O4	0.969 (19)	2.335 (18)	2.919 (2)	118.1 (13)
C20—H20B···O4	0.98 (2)	2.52 (2)	3.275 (2)	133.7 (15)
C11—H11A···O3 ⁱ	1.026 (19)	2.486 (19)	3.262 (2)	131.8 (13)
C17—H17A···O6 ⁱⁱ	0.98 (2)	2.53 (2)	3.219 (2)	127.0 (15)
C19—H19B···O3 ⁱⁱⁱ	0.90 (3)	2.51 (3)	3.157 (2)	129 (2)

Symmetry codes: (i) $x - 1, y, z$; (ii) $x + 1, y, z$; (iii) $-x + 2, y + \frac{1}{2}, -z + \frac{3}{2}$.

In a continuation of our research work devoted to the syntheses and crystal structures of quinoline derivatives (Bouzian *et al.*, 2019a), we report herein the molecular and crystal structures, Hirshfeld surface analysis, DFT and molecular docking investigation of 2-(2-oxo-1,3-oxazolidin-3-yl)ethyl 2-[2-(2-oxo-1,3-oxazolidin-3-yl)ethoxy]quinoline-4-carboxylate.

2. Structural commentary

In the title molecule (Fig. 1), the phenyl and pyridine rings of the quinoline system are slightly bent, with a dihedral angle between their mean planes of $3.47 (7)^\circ$. The oxazolidine ring (N2/O2/C12–C14) adopts an envelope conformation, with puckering parameters of $Q(2) = 0.112 (2) \text{ \AA}$ and $\varphi(2) = 115.3 (10)^\circ$. The C14 atom is at the envelope flap position, and it deviates from the least-square plane through the remaining four atoms by $0.070 (2) \text{ \AA}$. The other oxazolidine ring (N3/O7/C18–C20) has a twisted conformation along the C20–C19 bond, with puckering parameters $Q(2) = 0.1732 (18) \text{ \AA}$ and $\varphi(2) = 299.7 (6)^\circ$. The dihedral angles between the mean planes of the oxazolidine rings and the quinoline ring systems are $38.04 (9)^\circ$ for (N2/O2/C12–C14) and $57.34 (8)^\circ$ for (N3/

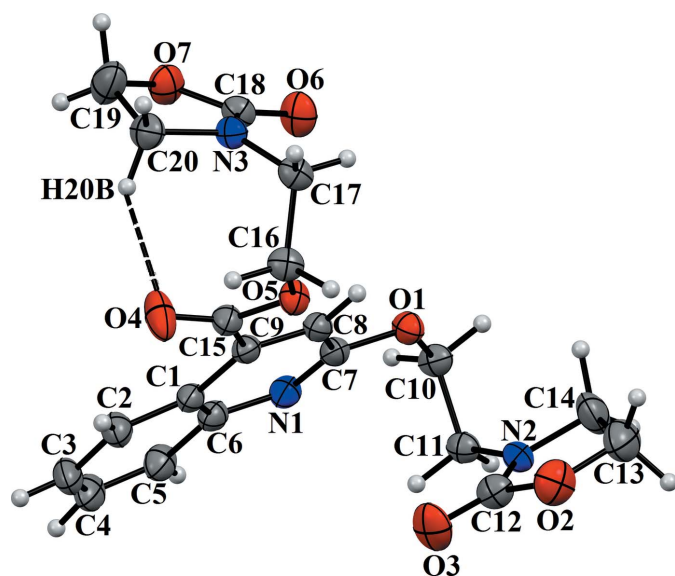


Figure 1
The molecular structure of the title compound, with atom labelling. Displacement ellipsoids are drawn at the 50% probability level. The intramolecular hydrogen bond is indicated by a dashed line.

O7/C18–C20). The molecular conformation is stabilized by an intramolecular C20—H20B···O4 contact (Fig. 1, Table 1), producing an $S(8)$ ring motif.

3. Supramolecular features

In the crystal, C11—H11A···O3ⁱ and C17—H17A···O6ⁱⁱ hydrogen bonds between methylene groups and carbonyl O atoms as well as C19—H19B···O3ⁱⁱⁱ hydrogen bonds lead to the formation of corrugated layers extending parallel to (001) (Fig. 2, Table 1). Notable C—H··· π and π – π interactions are not observed.

4. Database survey

A search of the Cambridge Structural Database (CSD, version 5.40, update of August 2019; Groom *et al.*, 2016) using ethyl quinoline-4-carboxylate as the main skeleton revealed the presence of ten structures with different substituents on the quinoline ring. The three structures most similar to the title compound are ethyl 2-(2,4,5-trimethoxyphenyl)quinoline-4-carboxylate (OJAGUD; Shrunghesh Kumar *et al.*, 2015), ethyl 2-(3,5-difluorophenyl)quinoline-4-carboxylate (UHUHAI; Sunitha *et al.*, 2015) and ethyl 6-chloro-2-ethoxyquinoline-4-carboxylate (XOFGAD; Bouzian *et al.*, 2019b). In OJAGUD, the dihedral angle between the quinoline ring system (r.m.s. deviation = 0.028 \AA) and the trimethoxybenzene ring is $43.38 (5)^\circ$. A short intramolecular C—H···O contact closes an $S(6)$ ring. In the crystal structure, inversion dimers linked by pairs of weak C—H···O interactions generate $R_2^2(6)$ loops. In UHUHAI, the two rings of the quinoline system have a dihedral angle of $2.28 (8)^\circ$ between their mean planes. The plane of the attached benzene ring is inclined to the plane of the quinoline system by $7.65 (7)^\circ$. There is a short intramolecular C—H···O contact involving the carbonyl group. In XOFGAD, the molecule is essentially planar with the mean plane of the ethyl acetate group making a dihedral angle of $5.02 (3)^\circ$ with the ethyl 6-chloro-2-ethoxyquinoline mean plane. There is an intramolecular C—H···O hydrogen bond

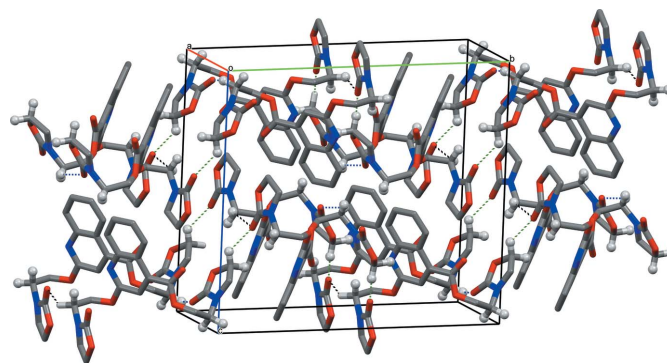
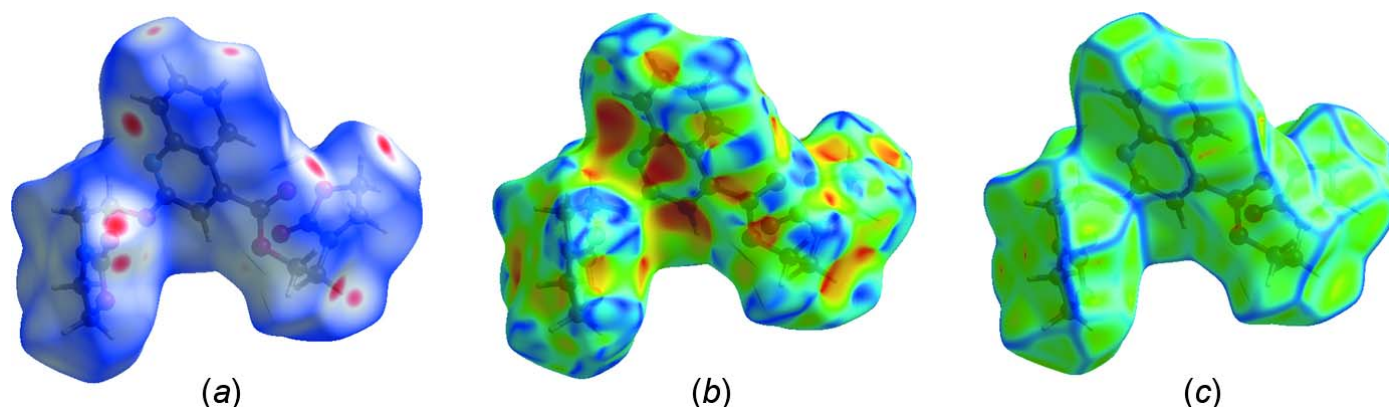


Figure 2
The crystal packing of the title compound, with C11—H11A···O3ⁱ, C17—H17A···O6ⁱⁱ and C19—H19B···O3ⁱⁱⁱ interactions shown as black, blue and green dashed lines, respectively.

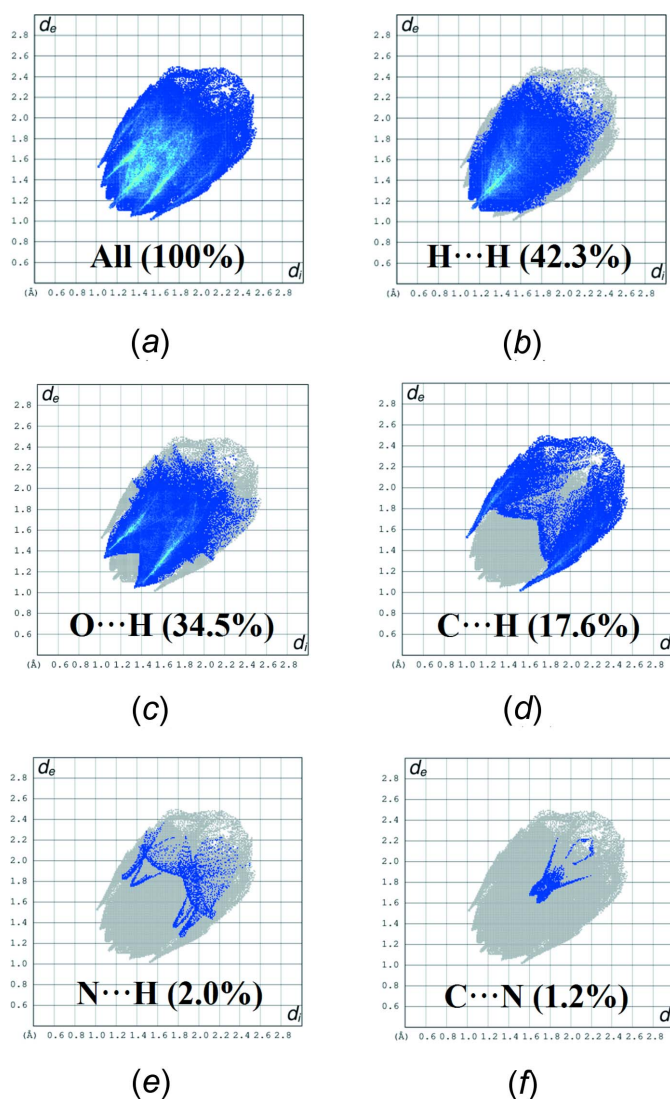

Figure 3

(a) d_{norm} mapped on the Hirshfeld surface to visualize the intermolecular interactions, (b) shape-index map of the title compound and (c) curvedness map of the title compound using a range from -4 to 4 Å.

forming an $S(6)$ graph-set motif. Weak intermolecular π - π interactions are observed in this crystal structure.

5. Hirshfeld surface analysis

Hirshfeld surface analysis was used to quantify the intermolecular contacts of the title compound, using *Crystal Explorer* (Turner *et al.*, 2017). The Hirshfeld surface was generated with a standard (high) surface resolution and with the three-dimensional d_{norm} surface plotted over a fixed colour scale of -0.1538 (red) to 1.1337 (blue) a.u. (Fig. 3a). The pale-red spots symbolize short contacts and negative d_{norm} values on the surface and correspond to the C-H...O interactions (Table 1). The shape-index map of the title molecule was generated in the range -1 to 1 Å (Fig. 3b). The convex blue regions symbolize hydrogen-donor groups and the concave red regions hydrogen-acceptor groups. The absence of adjacent red and blue triangles in the shape-index map, which generally indicate π - π interactions, reveals that this kind of interaction is not present in the title compound. The curvedness map was generated in the range -4.0 to 4.0 Å (Fig. 3c). It shows large regions of green with a relatively flat (*i.e.* planar) surface area while the blue regions demonstrate areas of curvature. The overall two-dimensional fingerprint plot is illustrated in Fig. 4a, with those delineated into H...H, H...O/O...H, H...C/C...H, H...N/N...H and C...N/N...C contacts associated with their relative contributions to the Hirshfeld surface given in Fig. 4a-f, respectively. The most important intermolecular interactions are H...H, contributing 42.3% to the overall crystal packing. H...O/O...H contacts arising from intermolecular C-H...O hydrogen bonding (Table 1) make a 34.5% contribution to the Hirshfeld surface and are represented by a pair of sharp spikes in the region $d_e + d_i \sim 2.35$ Å (Fig. 4c). The pair of wings in the fingerprint plot delineated into H...C/C...H contacts (17.6% contribution to the Hirshfeld surface) have a nearly symmetrical distribution of points, with the tips at $d_e + d_i \sim 2.54$ Å. The contributions of the other contacts to the Hirshfeld surface are negligible, *i.e.* H...N/N...H of 2.0% and C...N/N...C of 1.2%.


Figure 4

The full two-dimensional fingerprint plots for the title compound, showing (a) all interactions, and delineated into (b) H...H, (c) H...O/O...H, (d) H...C/C...H, (e) H...N/N...H and (f) C...N/N...C interactions.

Table 2
Calculated frontier molecular orbital energies (eV).

FMO	Energy
$E(\text{HOMO})$	-6.2102
$E(\text{LUMO})$	-1.9195
Energy gap (ΔE)	4.2907
Ionization potential (IP)	6.2102
Electron affinity (EA)	1.9195
Chemical potential (μ)	-4.0649
Electronegativity (χ)	4.0649
Chemical hardness (η)	2.1454
Chemical softness (σ)	0.2331
Electrophilicity index (ω)	3.8509

6. Frontier molecular orbital analyses

The energy levels for the title compound were computed on basis of density functional theory (DFT) using the standard B3LYP functional and 6-311G++ (d,p) basis-set calculations (Becke, 1993) as implemented in *GAUSSIAN 09* (Frisch *et al.*, 2009). The HOMO (highest occupied molecular orbital) acts as an electron donor and the LUMO (lowest occupied molecular orbital) as an electron acceptor. The energy levels, energy gaps, the ionization potential (IP), electron affinity (EA), the chemical potential (μ), the electronegativity (χ), chemical hardness (η), chemical softness (σ), and the electrophilicity index (ω) are given in Table 2. The electron transition from the HOMO to the LUMO energy level is shown in Fig. 5. If a molecule has a large HOMO–LUMO energy gap, it can be considered as hard with a low polarizability and a low chemical reactivity. Based on the numerical values collated in Table 2, the title compound can be classified as a hard material with a HOMO–LUMO energy gap of 4.2907 eV.

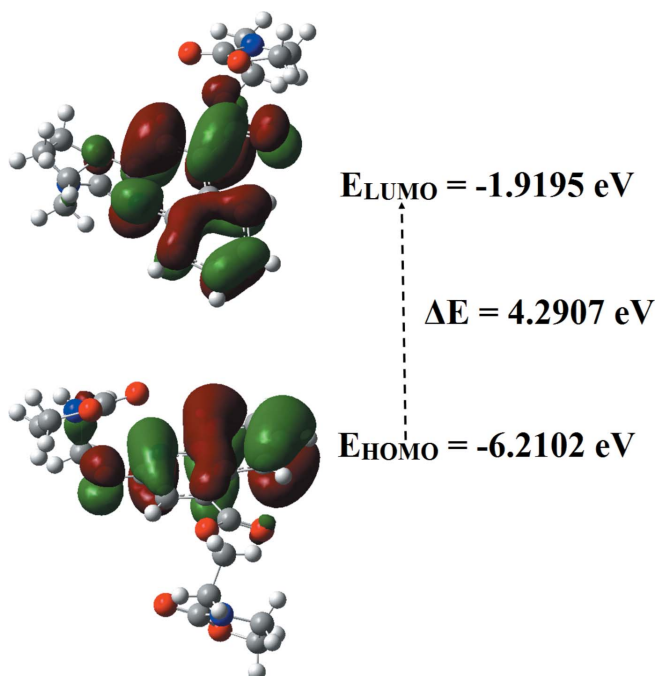


Figure 5
Molecular orbital energy levels of the title compound.

Table 3
The list of binding affinities and r.m.s.d. values of different sites in protein (6LU7) of the title compound.

Ligand	Affinity (kcal mol ⁻¹)	r.m.s.d./ub	r.m.s.d./lb
6LU7_ligand	-6.3	0.0	0.0
6LU7_ligand	-6.1	4.8	2.164
6LU7_ligand	-5.8	20.521	17.722
6LU7_ligand	-5.7	20.874	18.477
6LU7_ligand	-5.7	20.28	17.737
6LU7_ligand	-5.6	21.789	19.301
6LU7_ligand	-5.6	20.948	18.265
6LU7_ligand	-5.5	21.63	19.349
6LU7_ligand	-5.4	21.972	19.381

7. Molecular electrostatic potentials

The molecular electrostatic potential (MEP) map (Fig. 6) was calculated at the B3LYP/6-311G++ (d,p) level of theory. In the MEP diagram, the molecular electrostatic potential is in the range $-7.122 e^{-2}$ to $7.122 e^{-2}$, and the different electrostatic potentials at the surface of the molecule are represented by different colours. Electrostatic potentials increase in the order of red < yellow < green < blue, and red indicates the electron-rich region and blue indicates the electron-deficient region. As shown in Fig. 6, the carbonyl groups are surrounded by negative charges, indicating some possible nucleophilic attack sites. In addition, the positive charge regions are located on the H atoms.

8. Molecular docking study

A molecular docking study was performed to determine possible intermolecular interactions between the COVID-19 main protease (PDB ID: 6LU7) and the title molecule. The crystal structure of COVID-19 main protease in a complex with an inhibitor N3 was taken from the RSCB Protein Data Bank (PDB ID: 6LU7; Jin *et al.*, 2020). The molecular docking

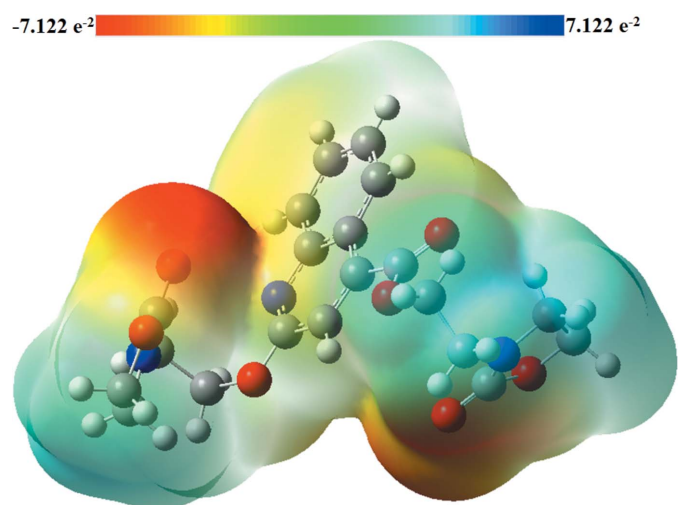


Figure 6
Theoretical molecular electrostatic potential surface calculated at the DFT/B3LYP/6-311 G++ (d,p) basis set level.

Table 4

The intermolecular hydrogen-bonding interactions with the distances (Å) between the title molecule and the macromolecule 6LU7.

Residue group	Ligand group	Distance	Hydrogen bond
NH ₃ group in LYS102	O atom in ethyl acetate	2.55	Conventional
NH ₂ group in GLN110	O atom in oxazolidine	2.55	Conventional
NH group in THR111	O atom in oxazolidine	1.92	Conventional
OH group in THR111	O atom in oxazolidine	2.28	Conventional
O atom in THR111	CH ₂ group in 1-methoxypropane	3.55	Carbon
NH ₂ group in ASN151	O atom in 1-methoxypropane	2.71	Conventional
O atom in ASP153	CH ₂ group in ethyl acetate	2.79	Carbon
OH group in SER158	O atom in ethyl acetate	2.12	Conventional
OH group in SER158	O atom in oxazolidine	2.60	Conventional

study was carried out using *PyRx AutoDock Vina Wizard*. The intermolecular interactions between the title compound and the target protein were visualized by using the *Discovery Studio 2020 Client* program (Biovia, 2017). The active sites of this target protein are residues LYS102, VAL104, GLN110, THR111, ASN151, ASP153 and SER158. Grid box sizes were determined as 25 × 25 × 25 Å³ and *x*, *y*, *z* centers: −10.865636, 12.146782, and 68.902236. The binding affinity energy values and their r.m.s.d. (root-mean-square deviation) values for nine different poses of the ligand docked onto receptor 6LU7 are listed in Table 3. According to the affinity binding energies, the best binding was determined with −6.3 (kcal mol^{−1}) energy and nine active hydrogen-bonding sites. The 2D and 3D visuals of the intermolecular interactions for the best binding pose of the title compound docked into macromolecule 6LU7 can be seen in Fig. 7. Table 4 lists details of intermolecular hydrogen-bonding interactions between the title molecule and the macromolecule 6LU7. Additionally in Fig. 7, π–σ and alkyl interactions and their bonding distances are shown. The title molecule appears to be a good agent because of its affinity and ability to adhere to the active sites of the protein.

9. Synthesis and crystallization

A solution of 0.8 g (4.23 mmol) of 2-oxo-1,2-dihydroquinoline-4-carboxylic acid in 30 ml of DMF was mixed with

1.5 g (8.46 mmol) bis(2-chloroethyl)amine hydrochloride, 2.33 g (16.92 mmol) K₂CO₃ and 0.13 g (0.423 mmol) tetra-*n*-butylammonium bromide (TBAB). The reaction mixture was stirred at 363 K for 9 h in DMF. After removal of formed salts by filtration, DMF was evaporated under reduced pressure, and the residue obtained was dissolved in dichloromethane. The organic phase was dried over Na₂SO₄ and then concentrated *in vacuo*. The resulting mixture was chromatographed on a silica gel column [eluent: ethyl acetate/hexane (2/8 v/v)]. Colourless single crystals of the title compound were obtained by slow evaporation of an ethanol solution.

10. Refinement

Crystal data, data collection and structure refinement details are summarized in Table 5. Hydrogen atoms were discernible from difference Fourier maps and were refined freely.

Funding information

The support of NSF–MRI grant No. 1228232 for the purchase of the diffractometer and Tulane University for support of the Tulane Crystallography Laboratory are gratefully acknowledged.

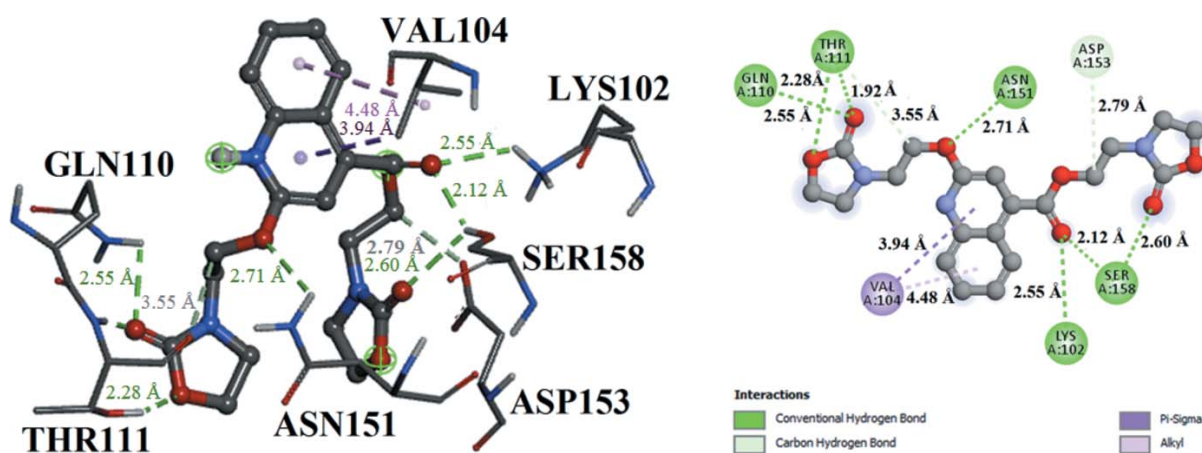


Figure 7

Three- and two-dimensional visuals of the intermolecular interactions for the best binding pose of the title compound docking with the residues of macromolecule 6LU7.

Table 5
Experimental details.

Crystal data	
Chemical formula	C ₂₀ H ₂₁ N ₃ O ₇
<i>M_r</i>	415.40
Crystal system, space group	Monoclinic, <i>P</i> 2 ₁ / <i>c</i>
Temperature (K)	150
<i>a</i> , <i>b</i> , <i>c</i> (Å)	6.0686 (5), 19.2791 (15), 16.3795 (13)
β (°)	94.185 (4)
<i>V</i> (Å ³)	1911.2 (3)
<i>Z</i>	4
Radiation type	Cu <i>K</i> α
μ (mm ⁻¹)	0.93
Crystal size (mm)	0.23 × 0.08 × 0.05
Data collection	
Diffractometer	Bruker D8 VENTURE PHOTON 100 CMOS
Absorption correction	Multi-scan (<i>SADABS</i> ; Krause <i>et al.</i> , 2015)
No. of measured, independent and observed [<i>I</i> > 2 σ (<i>I</i>)] reflections	14512, 3711, 3072
<i>R</i> _{int}	0.042
(<i>sin</i> θ / λ) _{max} (Å ⁻¹)	0.618
Refinement	
<i>R</i> [<i>F</i> ² > 2 σ (<i>F</i> ²)], <i>wR</i> (<i>F</i> ²), <i>S</i>	0.038, 0.094, 1.05
No. of reflections	3711
No. of parameters	356
H-atom treatment	All H-atom parameters refined
$\Delta\rho_{\text{max}}$, $\Delta\rho_{\text{min}}$ (e Å ⁻³)	0.22, -0.19

Computer programs: *APEX3* and *SAINT* (Bruker, 2016), *SHELXT* (Sheldrick, 2015a), *SHELXL2018/1* (Sheldrick, 2015b), *Mercury* (Macrae *et al.*, 2020), *PLATON* (Spek, 2020) and *pubCIF* (Westrip, 2010).

References

Becke, A. D. (1993). *J. Chem. Phys.* **98**, 5648–5652.
 Biovia (2017). *Discovery studio visualizer*. Vol. 936. Biovia, San Diego, CA, USA.
 Bouzian, Y., Faizi, M. S. H., Mague, J. T., Otmani, B. E., Dege, N., Karrouchi, K. & Essassi, E. M. (2019a). *Acta Cryst.* **E75**, 980–983.
 Bouzian, Y., Karrouchi, K., Anouar, E. H., Bouhfid, R., Arshad, S. & Essassi, E. M. (2019b). *Acta Cryst.* **E75**, 912–916.
 Bouzian, Y., Karrouchi, K., Sert, Y., Lai, C.-H., Mahi, L., Ahabchane, N. H., Talbaoui, A., Mague, J. T. & Essassi, E. M. (2020). *J. Mol. Struct.* **1209**, 127940.
 Bruker (2016). *APEX3* and *SAINT*. Bruker AXS, Inc., Madison, Wisconsin, USA.
 Chu, X. M., Wang, C., Liu, W., Liang, L. L., Gong, K. K., Zhao, C. Y. & Sun, K. L. (2019). *Eur. J. Med. Chem.* **161**, 101–117.
 Douche, D., Elmsellem, H., Anouar, E. H., Guo, L., Hafez, B., Tüzün, B., El Louzi, A., Bougrin, K., Karrouchi, K. & Himmi, B. (2020). *J. Mol. Liq.* **308**, 113042.

Frisch, M. J., Trucks, G. W., Schlegel, H. B., Scuseria, G. E., Robb, M. A., Cheeseman, J. R., Scalmani, G., Barone, V., Mennucci, B., Petersson, G. A., Nakatsuji, H., Caricato, M., Li, X., Hratchian, H. P., Izmaylov, A. F., Bloino, J., Zheng, G., Sonnenberg, J. L., Hada, M., Ehara, M., Toyota, K., Fukuda, R., Hasegawa, J., Ishida, M., Nakajima, T., Honda, Y., Kitao, O., Nakai, H., Vreven, T., Montgomery, J. A. Jr, Peralta, J. E., Ogliaro, F., Bearpark, M., Heyd, J. J., Brothers, E., Kudin, K. N., Staroverov, V. N., Kobayashi, R., Normand, J., Raghavachari, K., Rendell, A., Burant, J. C., Iyengar, S. S., Tomasi, J., Cossi, M., Rega, N., Millam, J. M., Klene, M., Knox, J. E., Cross, J. B., Bakken, V., Adamo, C., Jaramillo, J., Gomperts, R., Stratmann, R. E., Yazyev, O., Austin, A. J., Cammi, R., Pomelli, C., Ochterski, J. W., Martin, R. L., Morokuma, K., Zakrzewski, V. G., Voth, G. A., Salvador, P., Dannenberg, J. J., Dapprich, S., Daniels, A. D., Farkas, O., Foresman, J. B., Ortiz, J. V., Cioslowski, J. & Fox, D. J. (2009). *GAUSSIAN09*. Rev. A.02. Gaussian Inc., Wallingford, CT, USA.
 Gao, J., Tian, Z. & Yang, X. (2020). *Biosci. Trends*, **14**, 72–73.
 Groom, C. R., Bruno, I. J., Lightfoot, M. P. & Ward, S. C. (2016). *Acta Cryst.* **B72**, 171–179.
 Hu, Y. Q., Gao, C., Zhang, S., Xu, L., Xu, Z., Feng, L. S., Wu, X. & Zhao, F. (2017). *Eur. J. Med. Chem.* **139**, 22–47.
 Jin, Z., Du, X., Xu, Y., Deng, Y., Liu, M., Zhao, Y., Zhang, B., Li, X., Zhang, L., Peng, C., Duan, Y., Yu, J., Wang, L., Yang, K., Liu, F., Jiang, R., Yang, X., You, T., Liu, X., Yang, X., Bai, F., Liu, H., Liu, X., Guddat, L. W., Xu, W., Xiao, G., Qin, C., Shi, Z., Jiang, H., Rao, Z. & Yang, H. (2020). *Nature*, **582**, 289–293.
 Krause, L., Herbst-Irmer, R., Sheldrick, G. M. & Stalke, D. (2015). *J. Appl. Cryst.* **48**, 3–10.
 Macrae, C. F., Sovago, I., Cottrell, S. J., Galek, P. T. A., McCabe, P., Pidcock, E., Platings, M., Shields, G. P., Stevens, J. S., Towler, M. & Wood, P. A. (2020). *J. Appl. Cryst.* **53**, 226–235.
 Palit, P., Paira, P., Hazra, A., Banerjee, S., Gupta, A. D., Dastidar, S. G. & Mondal, N. B. (2009). *Eur. J. Med. Chem.* **44**, 845–853.
 Pinz, M., Reis, A. S., Duarte, V., da Rocha, M. J., Goldani, B. S., Alves, D., Savegnago, L., Luchese, C. & Wilhelm, E. A. (2016). *Eur. J. Pharmacol.* **780**, 122–128.
 Sheldrick, G. M. (2015a). *Acta Cryst.* **A71**, 3–8.
 Sheldrick, G. M. (2015b). *Acta Cryst.* **C71**, 3–8.
 Shrngesh Kumar, T. O., Naveen, S., Kumara, M. N., Mahadevan, K. M. & Lokanath, N. K. (2015). *Acta Cryst.* **E71**, o514–o515.
 Spek, A. L. (2020). *Acta Cryst.* **E76**, 1–11.
 Sunitha, V. M., Naveen, S., Manjunath, H. R., Benaka Prasad, S. B., Manivannan, V. & Lokanath, N. K. (2015). *Acta Cryst.* **E71**, o341–o342.
 Tang, Q. D., Duan, Y. L., Xiong, H. H., Chen, T., Xiao, Z., Wang, L. X., Xiao, Y. Y., Huang, S. M., Xiong, Y., Zhu, W., Gong, P. & Zheng, P. (2018). *Eur. J. Med. Chem.* **158**, 201–213.
 Turner, M. J., McKinnon, J. J., Wolff, S. K., Grimwood, D. J., Spackman, P. R., Jayatilaka, D. & Spackman, M. A. (2017). *CrystalExplorer17*. University of Western Australia. <http://hirshfeldsurface.net>.
 Westrip, S. P. (2010). *J. Appl. Cryst.* **43**, 920–925.
 Xu, Z., Gao, C., Ren, Q. C., Song, X. F., Feng, L. S. & Lv, Z. S. (2017). *Eur. J. Med. Chem.* **139**, 429–440.

supporting information

Acta Cryst. (2021). E77, 28-33 [https://doi.org/10.1107/S2056989020015960]

Crystal structure, Hirshfeld surface analysis, DFT and molecular docking investigation of 2-(2-oxo-1,3-oxazolidin-3-yl)ethyl 2-[2-(2-oxo-1,3-oxazolidin-3-yl)ethoxy]quinoline-4-carboxylate

Younos Bouzian, Cemile Baydere, Necmi Dege, Noureddine Hamou Ahabchane, Joel T. Mague, Abdulmalik Abudunia, Khalid Karrouchi and El Mokhtar Essassi

Computing details

Data collection: *APEX3* (Bruker, 2016); cell refinement: *SAINTE* (Bruker, 2016); data reduction: *SAINTE* (Bruker, 2016); program(s) used to solve structure: *SHELXT* (Sheldrick, 2015a); program(s) used to refine structure: *SHELXL2018/1* (Sheldrick, 2015b); molecular graphics: *Mercury* (Macrae *et al.*, 2020) and *PLATON* (Spek, 2020); software used to prepare material for publication: *publCIF* (Westrip, 2010).

2-(2-Oxo-1,3-oxazolidin-3-yl)ethyl 2-[2-(2-oxo-1,3-oxazolidin-3-yl)ethoxy]quinoline-4-carboxylate

Crystal data

$C_{20}H_{21}N_3O_7$

$M_r = 415.40$

Monoclinic, $P2_1/c$

$a = 6.0686$ (5) Å

$b = 19.2791$ (15) Å

$c = 16.3795$ (13) Å

$\beta = 94.185$ (4)°

$V = 1911.2$ (3) Å³

$Z = 4$

$F(000) = 872$

$D_x = 1.444$ Mg m⁻³

Cu $K\alpha$ radiation, $\lambda = 1.54178$ Å

Cell parameters from 9277 reflections

$\theta = 3.6$ – 72.3 °

$\mu = 0.93$ mm⁻¹

$T = 150$ K

Column, colourless

$0.23 \times 0.08 \times 0.05$ mm

Data collection

Bruker D8 VENTURE PHOTON 100 CMOS diffractometer

Radiation source: INCOATEC I μ S micro-focus source

Detector resolution: 10.4167 pixels mm⁻¹

ω scans

Absorption correction: multi-scan (*SADABS*; Krause *et al.*, 2015)

14512 measured reflections

3711 independent reflections

3072 reflections with $I > 2\sigma(I)$

$R_{int} = 0.042$

$\theta_{max} = 72.3$ °, $\theta_{min} = 3.6$ °

$h = -7 \rightarrow 6$

$k = -21 \rightarrow 23$

$l = -20 \rightarrow 18$

Refinement

Refinement on F^2

Least-squares matrix: full

$R[F^2 > 2\sigma(F^2)] = 0.038$

$wR(F^2) = 0.094$

$S = 1.05$

3711 reflections

356 parameters

0 restraints

Hydrogen site location: difference Fourier map

All H-atom parameters refined

$$w = 1/[\sigma^2(F_o^2) + (0.0346P)^2 + 0.6581P]$$

$$\text{where } P = (F_o^2 + 2F_c^2)/3$$

$$(\Delta/\sigma)_{\max} < 0.001$$

$$\Delta\rho_{\max} = 0.22 \text{ e } \text{\AA}^{-3}$$

$$\Delta\rho_{\min} = -0.19 \text{ e } \text{\AA}^{-3}$$

Extinction correction: SHELXL-2018/3

(Sheldrick 2015b),

$$F_c^* = kFc[1 + 0.001xFc^2\lambda^3/\sin(2\theta)]^{-1/4}$$

Extinction coefficient: 0.0026 (2)

Special details

Geometry. All esds (except the esd in the dihedral angle between two l.s. planes) are estimated using the full covariance matrix. The cell esds are taken into account individually in the estimation of esds in distances, angles and torsion angles; correlations between esds in cell parameters are only used when they are defined by crystal symmetry. An approximate (isotropic) treatment of cell esds is used for estimating esds involving l.s. planes.

Fractional atomic coordinates and isotropic or equivalent isotropic displacement parameters (\AA^2)

	x	y	z	$U_{\text{iso}}^*/U_{\text{eq}}$
O1	0.37759 (18)	0.21379 (5)	0.57549 (6)	0.0312 (3)
O2	0.7629 (2)	0.08767 (7)	0.44369 (8)	0.0493 (3)
O3	0.7633 (2)	0.07204 (8)	0.57987 (8)	0.0506 (3)
O4	1.1362 (2)	0.34395 (7)	0.75827 (7)	0.0530 (4)
O5	1.07647 (17)	0.32859 (5)	0.62287 (6)	0.0297 (2)
O6	0.68920 (19)	0.45136 (7)	0.59441 (7)	0.0426 (3)
O7	0.76696 (19)	0.50976 (7)	0.71190 (7)	0.0410 (3)
N1	0.4550 (2)	0.18848 (6)	0.71212 (8)	0.0307 (3)
N2	0.4425 (2)	0.08645 (7)	0.49889 (8)	0.0292 (3)
N3	1.0450 (2)	0.48184 (6)	0.63804 (8)	0.0284 (3)
C1	0.7992 (3)	0.23409 (7)	0.78094 (9)	0.0275 (3)
C2	0.9438 (3)	0.23392 (9)	0.85269 (10)	0.0355 (4)
C3	0.8913 (3)	0.19732 (9)	0.92045 (10)	0.0410 (4)
C4	0.6930 (3)	0.16004 (9)	0.92016 (10)	0.0409 (4)
C5	0.5501 (3)	0.15931 (9)	0.85188 (10)	0.0367 (4)
C6	0.6007 (3)	0.19519 (8)	0.78029 (9)	0.0295 (3)
C7	0.5068 (2)	0.21938 (7)	0.64584 (9)	0.0273 (3)
C8	0.6967 (3)	0.26216 (7)	0.63962 (9)	0.0270 (3)
C9	0.8405 (3)	0.27009 (7)	0.70638 (9)	0.0263 (3)
C10	0.2011 (3)	0.16344 (8)	0.57237 (10)	0.0316 (3)
C11	0.2925 (3)	0.09066 (8)	0.56362 (10)	0.0296 (3)
C12	0.6613 (3)	0.08141 (8)	0.51449 (10)	0.0343 (4)
C13	0.5965 (4)	0.09582 (12)	0.37669 (12)	0.0521 (5)
C14	0.3811 (4)	0.10463 (13)	0.41522 (11)	0.0503 (5)
C15	1.0341 (3)	0.31748 (8)	0.70093 (9)	0.0296 (3)
C16	1.2533 (3)	0.37628 (8)	0.60659 (10)	0.0307 (3)
C17	1.1579 (3)	0.44476 (8)	0.57658 (10)	0.0305 (3)
C18	0.8247 (2)	0.47778 (8)	0.64262 (9)	0.0293 (3)
C19	0.9624 (4)	0.54073 (12)	0.75294 (14)	0.0536 (5)
C20	1.1552 (3)	0.50923 (9)	0.71305 (11)	0.0368 (4)
H2	1.087 (3)	0.2562 (10)	0.8534 (10)	0.035 (5)*
H3	0.995 (4)	0.1973 (11)	0.9668 (13)	0.051 (6)*
H4	0.662 (3)	0.1323 (10)	0.9671 (12)	0.044 (5)*
H5	0.409 (3)	0.1320 (10)	0.8502 (12)	0.047 (5)*

H8	0.718 (3)	0.2863 (9)	0.5880 (11)	0.031 (4)*
H10A	0.104 (3)	0.1775 (9)	0.5222 (11)	0.033 (4)*
H10B	0.116 (3)	0.1663 (9)	0.6224 (11)	0.034 (4)*
H11A	0.158 (3)	0.0587 (9)	0.5522 (11)	0.037 (5)*
H11B	0.378 (3)	0.0759 (9)	0.6148 (11)	0.034 (5)*
H13A	0.593 (5)	0.0502 (15)	0.3426 (16)	0.084 (8)*
H13B	0.637 (5)	0.1344 (15)	0.3451 (17)	0.087 (9)*
H14A	0.267 (5)	0.0739 (14)	0.3906 (16)	0.075 (8)*
H14B	0.331 (5)	0.1581 (17)	0.4123 (17)	0.099 (10)*
H16A	1.355 (3)	0.3820 (9)	0.6562 (11)	0.031 (4)*
H16B	1.332 (3)	0.3535 (9)	0.5624 (11)	0.035 (5)*
H17A	1.281 (3)	0.4738 (10)	0.5615 (12)	0.044 (5)*
H17B	1.047 (3)	0.4375 (9)	0.5297 (11)	0.029 (4)*
H19A	0.942 (5)	0.5932 (16)	0.7433 (17)	0.092 (9)*
H19B	0.962 (4)	0.5331 (13)	0.8072 (17)	0.073 (8)*
H20A	1.268 (4)	0.5440 (13)	0.6998 (15)	0.068 (7)*
H20B	1.224 (3)	0.4711 (11)	0.7450 (12)	0.048 (5)*

Atomic displacement parameters (Å²)

	U^{11}	U^{22}	U^{33}	U^{12}	U^{13}	U^{23}
O1	0.0313 (6)	0.0295 (5)	0.0318 (6)	-0.0034 (4)	-0.0036 (4)	0.0011 (4)
O2	0.0420 (7)	0.0586 (8)	0.0491 (7)	-0.0029 (6)	0.0164 (6)	-0.0012 (6)
O3	0.0275 (6)	0.0764 (10)	0.0462 (7)	0.0044 (6)	-0.0090 (5)	-0.0006 (7)
O4	0.0718 (9)	0.0576 (8)	0.0280 (6)	-0.0357 (7)	-0.0071 (6)	0.0048 (6)
O5	0.0317 (6)	0.0320 (5)	0.0259 (5)	-0.0065 (4)	0.0062 (4)	0.0000 (4)
O6	0.0255 (6)	0.0581 (8)	0.0438 (7)	-0.0046 (5)	-0.0020 (5)	-0.0064 (6)
O7	0.0361 (7)	0.0504 (7)	0.0372 (6)	0.0060 (5)	0.0066 (5)	-0.0059 (5)
N1	0.0342 (7)	0.0287 (6)	0.0296 (7)	-0.0023 (5)	0.0055 (5)	-0.0018 (5)
N2	0.0276 (7)	0.0309 (7)	0.0284 (6)	0.0029 (5)	-0.0026 (5)	0.0007 (5)
N3	0.0232 (6)	0.0301 (6)	0.0316 (7)	-0.0013 (5)	-0.0009 (5)	-0.0002 (5)
C1	0.0368 (8)	0.0227 (7)	0.0233 (7)	-0.0003 (6)	0.0048 (6)	-0.0011 (5)
C2	0.0455 (10)	0.0336 (8)	0.0269 (8)	-0.0060 (7)	0.0000 (7)	0.0012 (6)
C3	0.0607 (12)	0.0382 (9)	0.0234 (8)	-0.0038 (8)	-0.0020 (7)	0.0022 (7)
C4	0.0638 (12)	0.0347 (8)	0.0252 (8)	-0.0061 (8)	0.0103 (8)	0.0022 (7)
C5	0.0480 (10)	0.0327 (8)	0.0307 (8)	-0.0067 (7)	0.0118 (7)	-0.0007 (6)
C6	0.0370 (9)	0.0257 (7)	0.0266 (7)	0.0001 (6)	0.0071 (6)	-0.0018 (6)
C7	0.0288 (8)	0.0244 (7)	0.0284 (7)	0.0020 (6)	0.0005 (6)	-0.0017 (6)
C8	0.0315 (8)	0.0245 (7)	0.0251 (7)	0.0019 (6)	0.0035 (6)	0.0012 (6)
C9	0.0326 (8)	0.0218 (7)	0.0250 (7)	-0.0002 (6)	0.0047 (6)	-0.0004 (5)
C10	0.0252 (8)	0.0298 (8)	0.0389 (9)	-0.0008 (6)	-0.0021 (7)	-0.0017 (7)
C11	0.0261 (8)	0.0292 (8)	0.0331 (8)	-0.0003 (6)	-0.0001 (6)	0.0016 (6)
C12	0.0285 (8)	0.0347 (8)	0.0399 (9)	-0.0005 (6)	0.0029 (7)	-0.0017 (7)
C13	0.0700 (14)	0.0514 (12)	0.0361 (10)	-0.0016 (10)	0.0106 (9)	0.0036 (9)
C14	0.0582 (13)	0.0632 (13)	0.0283 (9)	0.0099 (10)	-0.0041 (8)	0.0066 (8)
C15	0.0362 (9)	0.0264 (7)	0.0262 (7)	-0.0026 (6)	0.0029 (6)	0.0010 (6)
C16	0.0258 (8)	0.0319 (8)	0.0351 (8)	-0.0035 (6)	0.0071 (6)	0.0039 (6)
C17	0.0263 (8)	0.0339 (8)	0.0321 (8)	-0.0012 (6)	0.0062 (6)	0.0055 (6)

C18	0.0249 (8)	0.0328 (8)	0.0303 (8)	0.0008 (6)	0.0026 (6)	0.0033 (6)
C19	0.0502 (12)	0.0574 (13)	0.0509 (12)	0.0130 (10)	-0.0111 (9)	-0.0218 (10)
C20	0.0340 (9)	0.0346 (9)	0.0406 (9)	-0.0054 (7)	-0.0059 (7)	-0.0023 (7)

Geometric parameters (Å, °)

O1—C7	1.3499 (18)	C4—H4	0.97 (2)
O1—C10	1.4437 (19)	C5—C6	1.414 (2)
O2—C12	1.358 (2)	C5—H5	1.00 (2)
O2—C13	1.445 (3)	C7—C8	1.427 (2)
O3—C12	1.211 (2)	C8—C9	1.357 (2)
O4—C15	1.2006 (19)	C8—H8	0.982 (18)
O5—C15	1.3396 (18)	C9—C15	1.496 (2)
O5—C16	1.4526 (18)	C10—C11	1.519 (2)
O6—C18	1.2100 (19)	C10—H10A	1.013 (18)
O7—C18	1.3596 (19)	C10—H10B	1.001 (19)
O7—C19	1.449 (2)	C11—H11A	1.026 (19)
N1—C7	1.2969 (19)	C11—H11B	0.994 (19)
N1—C6	1.379 (2)	C13—C14	1.502 (3)
N2—C12	1.338 (2)	C13—H13A	1.04 (3)
N2—C14	1.437 (2)	C13—H13B	0.95 (3)
N2—C11	1.449 (2)	C14—H14A	0.98 (3)
N3—C18	1.347 (2)	C14—H14B	1.08 (3)
N3—C17	1.447 (2)	C16—C17	1.509 (2)
N3—C20	1.455 (2)	C16—H16A	0.992 (18)
C1—C2	1.415 (2)	C16—H16B	0.997 (18)
C1—C6	1.418 (2)	C17—H17A	0.98 (2)
C1—C9	1.443 (2)	C17—H17B	0.992 (18)
C2—C3	1.372 (2)	C19—C20	1.509 (3)
C2—H2	0.969 (19)	C19—H19A	1.03 (3)
C3—C4	1.401 (3)	C19—H19B	0.90 (3)
C3—H3	0.95 (2)	C20—H20A	0.99 (3)
C4—C5	1.364 (3)	C20—H20B	0.98 (2)
C7—O1—C10	117.84 (12)	C10—C11—H11B	110.9 (11)
C12—O2—C13	108.82 (14)	H11A—C11—H11B	109.8 (15)
C15—O5—C16	118.18 (12)	O3—C12—N2	128.04 (16)
C18—O7—C19	108.80 (13)	O3—C12—O2	122.28 (15)
C7—N1—C6	117.04 (13)	N2—C12—O2	109.68 (14)
C12—N2—C14	112.61 (15)	O2—C13—C14	105.94 (15)
C12—N2—C11	122.16 (13)	O2—C13—H13A	107.6 (15)
C14—N2—C11	123.44 (14)	C14—C13—H13A	109.5 (16)
C18—N3—C17	122.17 (13)	O2—C13—H13B	107.9 (17)
C18—N3—C20	111.80 (13)	C14—C13—H13B	114.0 (18)
C17—N3—C20	123.69 (13)	H13A—C13—H13B	112 (2)
C2—C1—C6	118.71 (14)	N2—C14—C13	101.55 (16)
C2—C1—C9	124.65 (14)	N2—C14—H14A	111.9 (15)
C6—C1—C9	116.63 (14)	C13—C14—H14A	111.7 (16)

C3—C2—C1	120.43 (16)	N2—C14—H14B	109.2 (15)
C3—C2—H2	118.6 (11)	C13—C14—H14B	110.1 (16)
C1—C2—H2	120.8 (10)	H14A—C14—H14B	112 (2)
C2—C3—C4	120.73 (17)	O4—C15—O5	123.69 (14)
C2—C3—H3	117.8 (13)	O4—C15—C9	125.14 (14)
C4—C3—H3	121.5 (13)	O5—C15—C9	111.15 (13)
C5—C4—C3	120.16 (15)	O5—C16—C17	110.03 (13)
C5—C4—H4	119.7 (12)	O5—C16—H16A	110.2 (10)
C3—C4—H4	120.0 (12)	C17—C16—H16A	111.8 (10)
C4—C5—C6	120.75 (16)	O5—C16—H16B	104.6 (11)
C4—C5—H5	121.2 (11)	C17—C16—H16B	110.0 (10)
C6—C5—H5	118.0 (11)	H16A—C16—H16B	109.9 (15)
N1—C6—C5	117.43 (15)	N3—C17—C16	113.29 (13)
N1—C6—C1	123.35 (13)	N3—C17—H17A	107.6 (12)
C5—C6—C1	119.20 (15)	C16—C17—H17A	107.4 (12)
N1—C7—O1	121.12 (14)	N3—C17—H17B	106.3 (10)
N1—C7—C8	124.86 (14)	C16—C17—H17B	110.5 (10)
O1—C7—C8	114.01 (13)	H17A—C17—H17B	111.9 (15)
C9—C8—C7	118.89 (14)	O6—C18—N3	128.17 (15)
C9—C8—H8	121.5 (10)	O6—C18—O7	122.10 (14)
C7—C8—H8	119.6 (10)	N3—C18—O7	109.72 (13)
C8—C9—C1	119.10 (14)	O7—C19—C20	105.53 (14)
C8—C9—C15	118.85 (13)	O7—C19—H19A	104.5 (16)
C1—C9—C15	122.03 (13)	C20—C19—H19A	114.5 (17)
O1—C10—C11	110.45 (12)	O7—C19—H19B	109.2 (17)
O1—C10—H10A	103.6 (10)	C20—C19—H19B	114.8 (17)
C11—C10—H10A	111.5 (10)	H19A—C19—H19B	108 (2)
O1—C10—H10B	111.0 (10)	N3—C20—C19	100.86 (14)
C11—C10—H10B	110.0 (10)	N3—C20—H20A	110.0 (14)
H10A—C10—H10B	110.3 (14)	C19—C20—H20A	113.2 (14)
N2—C11—C10	111.95 (13)	N3—C20—H20B	109.4 (12)
N2—C11—H11A	111.4 (10)	C19—C20—H20B	112.7 (12)
C10—C11—H11A	106.3 (10)	H20A—C20—H20B	110.3 (18)
N2—C11—H11B	106.5 (11)		
C6—C1—C2—C3	-0.7 (2)	C11—N2—C12—O3	8.8 (3)
C9—C1—C2—C3	-179.17 (16)	C14—N2—C12—O2	-6.6 (2)
C1—C2—C3—C4	-0.6 (3)	C11—N2—C12—O2	-171.89 (13)
C2—C3—C4—C5	0.5 (3)	C13—O2—C12—O3	177.93 (17)
C3—C4—C5—C6	0.8 (3)	C13—O2—C12—N2	-1.40 (19)
C7—N1—C6—C5	-177.44 (14)	C12—O2—C13—C14	8.3 (2)
C7—N1—C6—C1	0.5 (2)	C12—N2—C14—C13	11.2 (2)
C4—C5—C6—N1	175.98 (15)	C11—N2—C14—C13	176.20 (15)
C4—C5—C6—C1	-2.1 (2)	O2—C13—C14—N2	-11.2 (2)
C2—C1—C6—N1	-175.98 (14)	C16—O5—C15—O4	-1.1 (2)
C9—C1—C6—N1	2.7 (2)	C16—O5—C15—C9	177.08 (12)
C2—C1—C6—C5	2.0 (2)	C8—C9—C15—O4	158.27 (17)
C9—C1—C6—C5	-179.41 (13)	C1—C9—C15—O4	-20.1 (2)

C6—N1—C7—O1	177.84 (13)	C8—C9—C15—O5	-19.91 (19)
C6—N1—C7—C8	-3.2 (2)	C1—C9—C15—O5	161.75 (13)
C10—O1—C7—N1	-10.2 (2)	C15—O5—C16—C17	-103.49 (15)
C10—O1—C7—C8	170.70 (13)	C18—N3—C17—C16	-95.85 (17)
N1—C7—C8—C9	2.4 (2)	C20—N3—C17—C16	65.35 (19)
O1—C7—C8—C9	-178.56 (13)	O5—C16—C17—N3	66.50 (17)
C7—C8—C9—C1	1.1 (2)	C17—N3—C18—O6	-9.0 (3)
C7—C8—C9—C15	-177.26 (13)	C20—N3—C18—O6	-172.23 (16)
C2—C1—C9—C8	175.18 (15)	C17—N3—C18—O7	171.83 (13)
C6—C1—C9—C8	-3.4 (2)	C20—N3—C18—O7	8.61 (18)
C2—C1—C9—C15	-6.5 (2)	C19—O7—C18—O6	-175.41 (17)
C6—C1—C9—C15	174.97 (13)	C19—O7—C18—N3	3.81 (19)
C7—O1—C10—C11	-75.87 (16)	C18—O7—C19—C20	-13.9 (2)
C12—N2—C11—C10	105.84 (17)	C18—N3—C20—C19	-16.32 (19)
C14—N2—C11—C10	-57.8 (2)	C17—N3—C20—C19	-179.25 (16)
O1—C10—C11—N2	-48.92 (18)	O7—C19—C20—N3	17.5 (2)
C14—N2—C12—O3	174.08 (19)		

Hydrogen-bond geometry (\AA , $^\circ$)

$D-H\cdots A$	$D-H$	$H\cdots A$	$D\cdots A$	$D-H\cdots A$
C2—H2 \cdots O4	0.969 (19)	2.335 (18)	2.919 (2)	118.1 (13)
C20—H20B \cdots O4	0.98 (2)	2.52 (2)	3.275 (2)	133.7 (15)
C11—H11A \cdots O3 ⁱ	1.026 (19)	2.486 (19)	3.262 (2)	131.8 (13)
C17—H17A \cdots O6 ⁱⁱ	0.98 (2)	2.53 (2)	3.219 (2)	127.0 (15)
C19—H19B \cdots O3 ⁱⁱⁱ	0.90 (3)	2.51 (3)	3.157 (2)	129 (2)

Symmetry codes: (i) $x-1, y, z$; (ii) $x+1, y, z$; (iii) $-x+2, y+1/2, -z+3/2$.